

Identifying capacitive and inductive loss in lumped element superconducting hybrid titanium nitride/aluminum resonators

Michael R. Vissers, Martin P. Weides, Jeffrey S. Kline, Martin Sandberg, and David P. Pappas

Citation: [Applied Physics Letters](#) **101**, 022601 (2012); doi: 10.1063/1.4730389

View online: <http://dx.doi.org/10.1063/1.4730389>

View Table of Contents: <http://scitation.aip.org/content/aip/journal/apl/101/2?ver=pdfcov>

Published by the [AIP Publishing](#)

Articles you may be interested in

[Improved superconducting qubit coherence using titanium nitride](#)

Appl. Phys. Lett. **103**, 012602 (2013); 10.1063/1.4813269

[Etch induced microwave losses in titanium nitride superconducting resonators](#)

Appl. Phys. Lett. **100**, 262605 (2012); 10.1063/1.4729623

[Microwave-induced excess quasiparticles in superconducting resonators measured through correlated conductivity fluctuations](#)

Appl. Phys. Lett. **100**, 162601 (2012); 10.1063/1.4704151

[Substrate-dependent quasiparticle recombination time in superconducting resonators](#)

Appl. Phys. Lett. **99**, 062509 (2011); 10.1063/1.3624463

[Low-loss superconducting resonant circuits using vacuum-gap-based microwave components](#)

Appl. Phys. Lett. **96**, 093502 (2010); 10.1063/1.3304168

Agilent's Electronic Measurement Group is becoming **Keysight Technologies**.



Engineering Education & Research Resources DVD 2014

Agilent is the key to your test and measurement needs **Order yours**



The advertisement features a red header with the text 'Agilent's Electronic Measurement Group is becoming Keysight Technologies.' Below this is a row of ten colorful icons representing various engineering and research fields. The central focus is a DVD cover for 'Agilent Technologies Engineering Education & Research Resources DVD 2014'. The cover is blue and white with a grid of icons. To the right of the DVD cover is a large blue button with the text 'Order yours'. At the bottom of the advertisement is the Agilent Technologies logo, which consists of a stylized starburst icon followed by the company name.

Identifying capacitive and inductive loss in lumped element superconducting hybrid titanium nitride/aluminum resonators

Michael R. Vissers,^{a)} Martin P. Weides,^{b)} Jeffrey S. Kline, Martin Sandberg, and David P. Pappas^{c)}

National Institute of Standards and Technology, Boulder, Colorado 80305, USA

(Received 21 March 2012; accepted 7 June 2012; published online 9 July 2012)

We present a method to systematically locate and extract capacitive and inductive losses in superconducting resonators at microwave frequencies by use of mixed-material, lumped element devices. In these devices, ultra-low loss titanium nitride was progressively replaced with aluminum in the inter-digitated capacitor and meandered inductor elements. By measuring the power dependent loss at 50 mK as the Al/TiN fraction in each element is increased, we find that at low electric field, i.e., in the single photon limit, the loss is two level system in nature and is correlated with the amount of Al capacitance rather than the Al inductance. In the high electric field limit, the remaining loss is linearly related to the product of the Al area times its inductance and is likely due to quasiparticles generated by stray IR radiation. At elevated temperature, additional loss is correlated with the amount of Al in the inductance, with a power independent TiN-Al interface loss term that exponentially decreases as the temperature is reduced. The TiN-Al interface loss is vanishingly small at the 50 mK base temperature. [<http://dx.doi.org/10.1063/1.4730389>]

Superconducting resonators with low loss are of great interest for photon detection¹ and quantum computation.² Hybrid devices, using different materials in specific parts of the resonant circuit, allow the alteration of intrinsic materials properties such as the superconducting gap, radiation cross-section, and capacitive and inductive loss within the resonators to optimize the entire circuit. Locating whether the residual loss sources are inductive or capacitive in nature is of considerable relevance. So far, most resonator studies have been done on single films in either coplanar waveguide resonators (CPWs) or lumped element circuits.³⁻⁹ The distributed capacitive and inductive elements in CPWs complicate the analysis, including the interpretation and location of the measured resonator loss. More specifically, the loss contributions of the capacitive δ_C and inductive δ_L parts are inherently linked and cannot be investigated separately in distributed element devices like CPWs. Further, even in lumped element devices typically both the capacitor and the inductor are usually formed by the same material, with limited research done on mixed-material devices with interfaces. In this work, we address these issues by studying lumped element resonators with components of mixed materials. However, we note that the lumped element approach is an approximation, depending on the exact current and voltage distributions in the resonant circuit. Therefore we distinguish between and investigate the actual capacitive and inductive losses in the specific elements as each element has contributions from both.

In a resonator the energy stored is E_{total} , where on average the capacitive energy equals the inductive energy. The

measured resonator loss, $\delta_{\text{meas.}}$, is the measurement of the relative energy loss $\Delta E/E_{\text{total}}$ per cycle time and defined as

$$\delta_{\text{meas.}} = \frac{\Delta E}{2\pi E_{\text{total}}} = \frac{\Delta E_C + \Delta E_L}{2\pi E_{\text{total}}} = \delta_C + \delta_L. \quad (1)$$

The conventional resonator characterization is done by measuring the resonator loss and frequency under power and temperature sweeps respectively. The capacitive loss, δ_C , is believed to be due to the presence of two-level systems (TLSs)¹⁰ and is inferred from both the power dependent loss and resonance frequency temperature dependence, as reviewed in Ref. 11. The decreased loss at higher powers is naturally explained by TLS loss, which scales with the electric field, E , as

$$\delta_{\text{meas.}} \propto \frac{1}{\sqrt{1 + \left(\frac{E}{E_s}\right)^2}} + \delta_{\text{P.I.}}, \quad (2)$$

where E_s is a saturation electric field for TLS loss.¹⁰ In addition to TLS loss, there is also a power-independent background loss, $\delta_{\text{P.I.}}$, typically attributed to the inductive loss, δ_L , caused, for example, by quasiparticles or radiative loss. The power independent loss typically limits the total resonator loss, causing the measured loss' electric field dependence to deviate from $1/E$ at high electric fields.¹¹

In this paper, we present a complementary characterization method to determine the capacitive and inductive losses in resonators by use of lumped elements made up of different materials. Devices fabricated from different materials allow us to vary the T_c and the different microwave loss factors of the constituent components highlighting their contributions to the loss of the different circuit elements. We tested this approach using titanium nitride and aluminum on Si. In addition to having a $T_c = 4.5 - 5$ K, optimally grown TiN on Si

^{a)}Electronic mail: michael.vissers@NIST.gov.

^{b)}Current address: Karlsruhe Institute of Technology, 76131 Karlsruhe, Germany.

^{c)}Electronic mail: david.pappas@NIST.gov.

is one of the lowest loss resonator materials with $3 : 2 \mu\text{m}$ CPWs having a low electric field, low temperature, loss factor $\sim 1 \times 10^{-6}$, and high field loss $< 1 \times 10^{-7}$.⁸ Evaporated Al, used in qubits, e.g., Refs. 12 and 13, has a $T_c = 1.2 \text{ K}$. However when grown on Si, the oxide surface and intermixing at the substrate interface give rise to relatively high loss $\delta_{\text{int}} > 10^{-5}$,¹⁴ providing a contrast to the lower loss TiN. The lower superconducting gap in Al facilitates quasiparticle creation from elevated temperatures or infrared radiation.^{15,16} In addition to determining the capacitive and inductive loss contributions, we also probe the Al-TiN material interface, which has not been investigated in previous single layer studies. This interface appears to have a small, but non-zero contribution to the loss at elevated temperature, but is negligible at the base temperature. This work highlights the feasibility of engineered lumped element resonators made from two or more materials whose specific capacitive or inductive properties are optimally tuned to take advantage of the constituent elements.

For our devices, 100 nm thick TiN was first grown at 500°C on an intrinsic silicon wafer⁸ and patterned using optical lithography and a Cl based reactive ion etch. While fluorine etched and deeply trenched TiN resonators have one of the lowest loss factors,¹⁷ the chlorine etch chosen in this work gave a better defined silicon interface without trenches complicating the subsequent Al liftoff. However, the Cl based etch does cause slightly increased internal resonator loss of $\delta_{\text{int.}} \approx 5 \times 10^{-6}$.¹⁸ The exposed silicon surface was then radio frequency (RF) plasma cleaned before the aluminum evaporation. The RF treatment might increase the loss in the exposed silicon and TiN regions. Finally we deposited a 100 nm thick aluminum layer with e-beam evaporation which was patterned with a lift-off process. The Al film overlapped the TiN film forming $2 \mu\text{m} \times 2 \mu\text{m}$ contacts which were also RF cleaned to give a clean interface. The films were patterned into frequency multiplexed lumped element resonators with varying degrees of TiN and Al participation. The internal wiring and microwave measurement lines were made from TiN for all devices. The resonators were capacitively coupled to a microwave coplanar waveguide feedline, permitting the loss extraction from transmission measurements of the S_{21} parameters, and the internal loss of a specific resonator, $\delta_{\text{int.}}$, is given by

$$\delta_{\text{int.}} = \delta_{\text{meas.}} - \delta_{\text{coup.}}, \quad (3)$$

where $\delta_{\text{coup.}}$ is the loss due to the capacitive coupling to the feedline.

The resonators are formed by an inductor (meandered $2 \mu\text{m}$ wide wire with $2 \mu\text{m}$ gap) being symmetrically shunted by two inter-digitated capacitors (IDCs) ($2 \mu\text{m}$ wide fingers and gaps), see Fig. 1. The footprint per resonator is $400 \mu\text{m} \times 450 \mu\text{m}$. The superconductors' width and gap were chosen to be similar to the features in conventional coplanar waveguide resonators. One resonator electrode is galvanically connected to the ground plane formed by TiN. Around the resonator are flux holes in the ground plane to inhibit trapped vortices.¹⁹ This resonator design yields intrinsic loss factors similar to those measured on otherwise identical coplanar waveguide resonators. On the first design, the hybrid

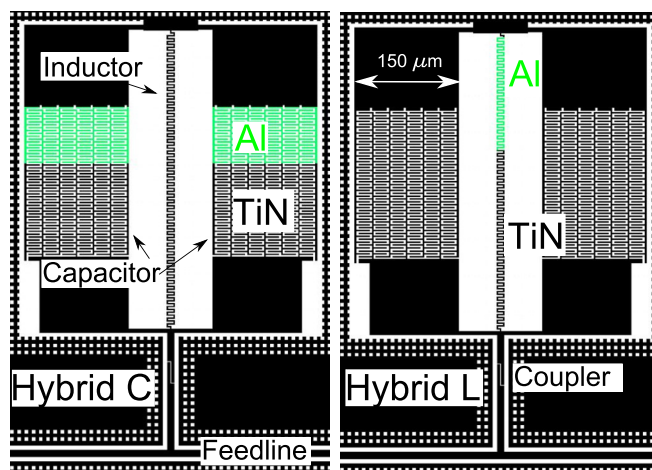


FIG. 1. Drawn resonator designs *hybrid capacitor* (left) and *hybrid inductor* (right) with $3 : 2$ TiN : Al fraction. The TiN (black) inter-digitated capacitors and meandered inductors are progressively replaced with Al (green). The frequency multiplexed resonators are capacitively coupled to the feedline.

capacitor device, the TiN capacitor was progressively replaced with Al while the inductor was formed by TiN. On the second design, the hybrid inductor device, the inductor had varied Al/TiN fractions, while the capacitor was always formed by TiN. Comparing simulations with our measurements of the resonant frequency for the different TiN fractions, we determined a kinetic inductance of 0.4 pH/square for the TiN film.

Illustrations of the resonator designs are shown in Fig. 1. Each design was integrated as frequency multiplexed resonators coupled to a common feedline. In total, for each design, we measured one all-TiN, one fully Al hybrid, and four mixed resonant elements with various Al/TiN fractions. The IDC capacitance was designed to be 600 fF , and the geometric meandered inductance was nominally 0.74 nH for the hybrid inductor devices. Frequency multiplexing of the resonators was a natural consequence of the kinetic inductance of the different TiN fraction. For the hybrid capacitor devices, the geometric inductances were varied ($0.64\text{--}0.86 \text{ nH}$). The self-capacitance of the inductor and inductance of the capacitor plays an important role in the loss of the entire structure. Using calculations from an electromagnetic field solver we estimate the self-capacitance of the meandered inductor as 18% of the total capacitance and the self-inductance of the IDC as about 3% of the total inductance. These calculations agree well with the measured resonance frequencies, f_r , of 5.5 and 6.9 GHz , though we obtain better fits if we assume the capacitor has 4% of the inductance. The resonator impedance is around $30\text{--}35 \Omega$.

The devices were measured in an adiabatic demagnetization refrigerator with a base temperature of 50 mK . The aluminum sample box holding the resonator chip was magnetically shielded with outer paramagnetic and inner niobium superconducting shields. The openings for the two microwave connectors were minimized to reduce incoming stray light. Measurements were performed with a vector network analyzer. The measurement chain was comprised of a combination of attenuators (room temperature and cold) and a low pass filter on the input line to achieve the appropriate

power level and eliminate radiation at the device input port (total attenuation -100 dB). On the output side of the sample box there was a microwave isolator and high- and low-pass filters before a high electron mobility transistor amplifier at the 4 K 2nd stage, with an additional room temperature amplifier. The power stored in the resonators was calculated in terms of both electric field and microwave photon numbers in the standard manner from the attenuation and measured resonance parameters.²⁰ Transmitted power measurements were taken as a function of frequency, power and temperature for all resonators. All traces were taken at low enough field such that the measured resonances remained symmetric. We measured over almost 4 decades of electric field (thus 7 decades in photon numbers) and at low temperature, i.e., with a base temperature T of 50 mK, and a resonance frequency of 6 GHz, $T < \hbar\omega_r/2k_B$ and the TLSs are not thermally saturated.

The electric field dependence of δ_{int} at 50 mK is shown in Fig. 2. The intrinsic loss, δ_{int} , is constant for low electric fields, before starting to drop off above the critical field. The loss is highest below the critical field, i.e., in the single photon regime, referred to here as $\delta(\text{SP})$, shown at about 1 V/m, due to the presence of unsaturated TLSs. The highest loss was observed for the hybrid device with the all-Al capacitor, with $\delta_c^{\text{Al}}(\text{SP}) = 55 \pm 5 \times 10^{-6}$, while the lowest loss was observed for the all-TiN devices, with $\delta^{\text{TiN}}(\text{SP}) = 5 \pm 1 \times 10^{-6}$. As expected, the loss curves of the hybrid Al-TiN devices fall between these two bounds.

An alternative method of determining loss due to TLSs is done with a temperature sweep. In this method, $\delta^{\text{TiN}}(\text{TLS})$ is extracted at high power from the resonant frequency shift with temperature. This occurs because the off-resonant TLSs become thermally saturated. However, this technique can only be used when there are no other temperature dependent

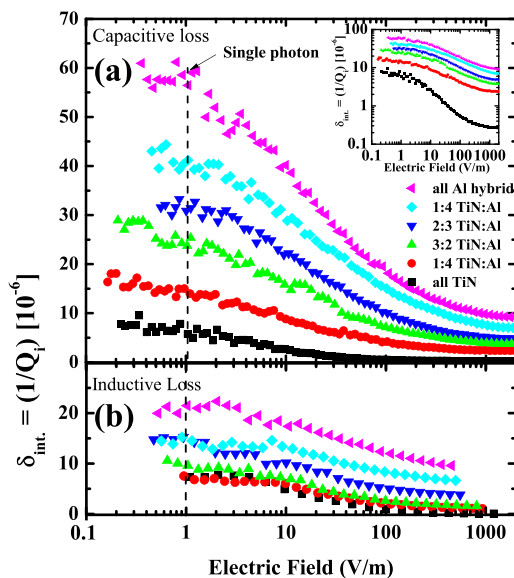


FIG. 2. Loss for (a) hybrid capacitor and (b) hybrid inductor resonators as a function of the electric field in the capacitor. The inset in (a) is the hybrid C loss plotted on a log scale to illustrate its characteristics at high power. The single photon levels are indicated. When Al is added to the capacitor, there is a greater increase in loss than if Al is added to the inductor. At higher fields the resonator loss reaches a minimum at an internal resonator power^{3,20} ≈ -40 dBm.

sources of loss, e.g., quasiparticles. In particular, for Al, a superconductor with a relatively low T_c , the underlying condition, $T \ll T_c$ with resonator temperature T , does not hold. Hence, we can only use this technique for the all-TiN resonator. From this measurement, we obtained $\delta_c^{\text{TiN}} \approx 5 \pm 1 \times 10^{-6}$, in agreement with the power-dependent loss shown in Fig. 2.

In quantum information applications, the very low electric field, i.e., single photon regime, loss is important. However, this measured loss is composed of both power dependent loss terms, e.g., TLSs, as well as any power independent loss arising from quasiparticles, etc. In order to separate these loss terms, we fit to the loss at the highest powers and subtract a constant loss such that the electric field dependence of loss matches Eq. (2), i.e., proportional to $1/E$.¹¹ We now have two loss terms, δ_{TLS} and $\delta_{\text{P.I.}}$, which we then can independently investigate the source of their loss.

If the TLS loss was solely in the inductor or capacitor, we would expect to only measure a change when Al is substituted in that element. However, the circuit is not composed of completely lumped elements and there is finite capacitance in the meandered inductor amounting to 18% of the total capacitance of the circuit. When the loss is plotted vs. Al capacitive fraction in Fig. 3(a), i.e., the 100% Al fraction hybrid C device has 82% Al capacitive fraction while the 100% Al fraction hybrid L device has 18% Al capacitive fraction, the extracted TLS losses for all devices show good agreement with a linear fit to the hybrid C data. The hybrid L devices do exhibit slightly less loss than expected from the fit; but while the meandered inductor has the same $2 \mu\text{m}$ spacing as the IDC, the exact electric field distribution and corresponding filling factor will be different for the meandered inductor versus the IDC and we should not expect perfect agreement. The fitted line from the hybrid Al devices closely intersects with the measured all-TiN devices indicating that any additional loss due to the TiN-Al interface is small, beneath the $\sim 1 \times 10^{-6}$ uncertainty in our measurement.

We also observe increased loss at high electric fields in devices that contain more Al. This loss is not related to just the percentage of Al capacitance or inductance in isolation. It fits better to the product of the Al inductance and area than to any single circuit parameter. The small amount of inductance in the IDCs, $\sim 4\%$ of the total, is compensated by their $17\times$ larger area than the meander. The relationship between the power independent loss at the lowest temperatures

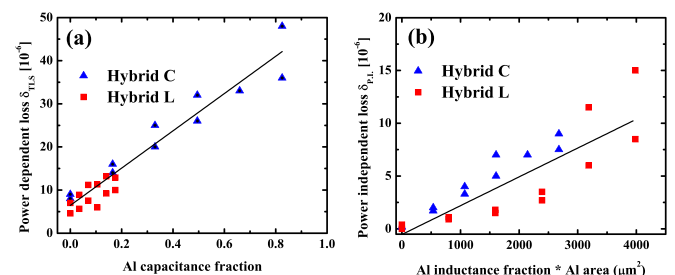


FIG. 3. (a) The power dependent loss δ_{TLS} at 50 mK bath temperature versus Al capacitive fraction. As the TiN is replaced by the Al in the hybrid L (square) or hybrid C (triangle) devices, additional power dependent loss is measured and agrees with a linear fit. (b) The power independent loss, $\delta_{\text{P.I.}}$, versus the product of the Al inductance fraction \times area.

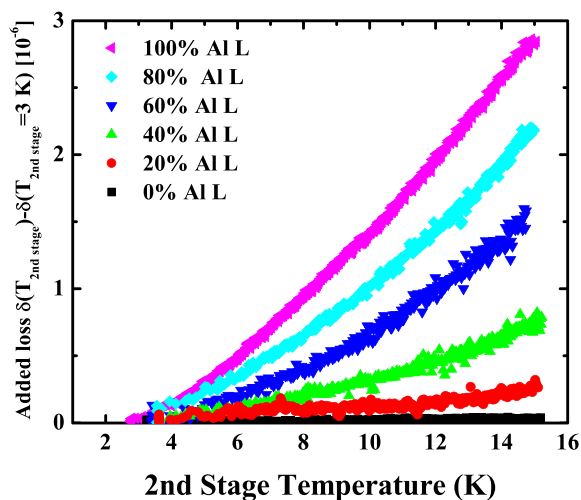


FIG. 4. The added loss measured in the hybrid L resonators as the 2nd stage temperature of the ADR is increased. The cold stage remains below 100 mK, which as shown in Fig. 5 does not add more loss. Greater loss is measured in devices which have larger Al percentages.

suggests that its source is likely due to quasiparticles generated by stray IR light emanating from the 4 K stage.^{15,16} This is further supported by our measurements with better absorptive materials inside the box that reduced the power-independent loss term by up to 50% for the all Al devices.

Furthermore, we made measurements similar to those first done by Baselmans²¹ to study the effect of IR radiation on the devices. The ADR pulse tube was turned off, and the 2nd stage was allowed to rise in temperature to 15 K over several minutes. During this time the FAA cold stage temperature remained below 100 mK implying that any additional thermal quasiparticle generation in the Al would be

minimal. As is shown in Fig. 4, increasing the 2nd stage temperature increased the measured loss in all devices containing Al, with greater loss correlated with greater Al percentage. The all-TiN device was practically unchanged, with the loss increasing by $<1 \times 10^{-7}$. While we cannot rule out the effect of microscopic roughness and morphology or fabrication damage, based on the similarity in the Al RF properties to other lightly shielded Al on Si measurements^{4,14} and the discussion above we believe that stray IR light is the dominant loss term contributing to the greater power independent loss in the Al hybrid devices.

The loss in the hybrid devices can also be studied as a function of temperature. In order to separate the temperature dependent loss from any potential TLS loss, the devices were measured at very high power where the TLS loss is saturated. The measured temperature dependent losses are shown in Fig. 5(a). As the temperature is increased in all devices, the loss rises exponentially. Devices with more Al have greater loss at all temperatures. This loss is enhanced when the Al is placed in the meandered inductor region. In Fig. 5(b), the loss at 0.5 K in both hybrid L and C devices is plotted and agrees with a linear fit to the percentage of Al's inductance in the circuit. As the temperature dependent loss is in the inductance, it is likely due to thermally activated quasiparticles in the Al.

While the loss in the hybrid C devices at any particular temperature increases with the amount of Al, at higher temperatures the slope of the measured temperature dependent loss vs Al percentage does not intercept the all TiN device at zero Al percentage, i.e. additional loss is measured whenever there exists an Al-TiN interface in the device. Figure 6(a) shows the temperature dependent loss vs Al fraction for the hybrid C devices at temperatures between 0.2 and 0.9 K.

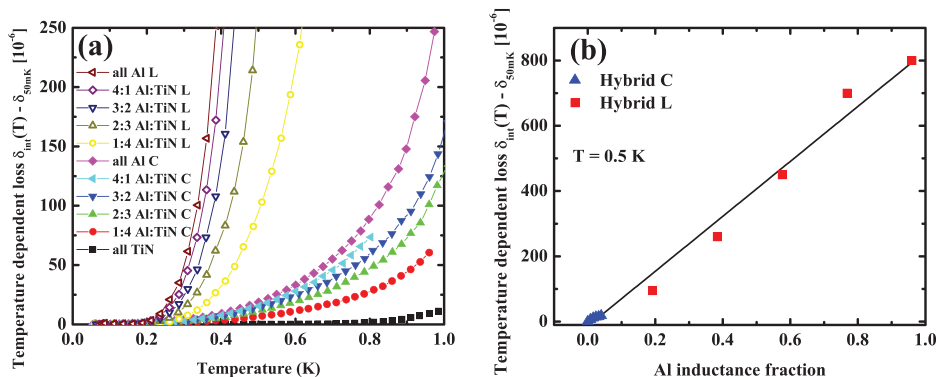


FIG. 5. (a) Temperature dependent loss $\delta_{\text{int}}(T) - \delta_{50\text{mK}}$ of the hybrid C (closed symbols) and hybrid L (open symbols) devices as a function of temperature. The devices are measured at high power and the 50 mK bath temperature loss is subtracted to reduce the contribution of any other loss terms. The lines are a guide to the eye. (b) The temperature dependent loss of all hybrid L and C resonators at 0.5 K versus Al inductance fraction agrees well to a linear fit.

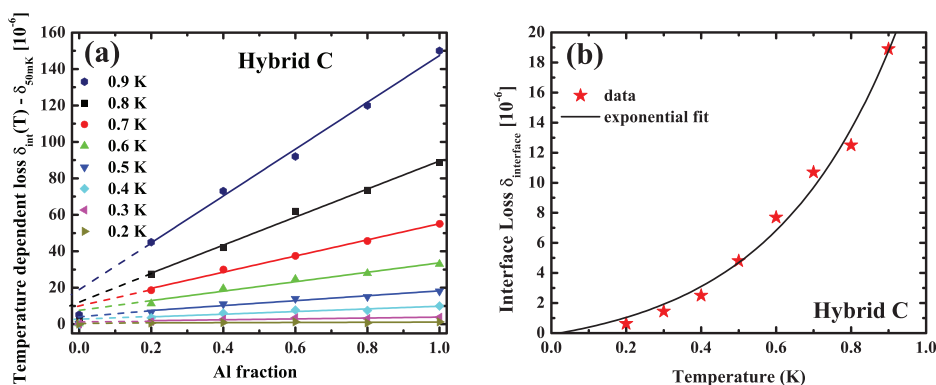


FIG. 6. (a) The temperature dependent loss $\delta_{\text{int}}(T) - \delta_{50\text{mK}}$ (symbols) in the hybrid C devices versus Al fraction at different temperatures between 0.2-0.9 K. In the hybrid capacitor devices the fit (solid lines) to the temperature dependent loss of the 5 hybrid devices with Al is linear in Al fraction at all temperatures, but the extrapolations of these fits (dashed lines) do not intersect with the loss from the pure TiN device. (b) The interface loss, $\delta_{\text{interface}}$, from the y-intercept from (a), plotted vs temperature with an exponential fit (solid line).

While the 5 devices with Al agree closely with linear fits (solid lines) to the Al fraction, the extrapolations of these fits (dashed lines) do not intersect with the measured loss of the all TiN resonator. This implies that there is a relatively small, but additional, loss term whenever any Al is incorporated into the circuit, corresponding to the existence of interfaces between the Al and the TiN. This interfacial or excess loss corresponding to the presence of Al, increases with temperature and is plotted in Fig. 6(b) along with an exponential fit the data. The exponential increase in loss with temperature suggests quasiparticles, and the activation energy scale is similar to the TiN superconducting gap energy, though this interface loss is much greater than the measured temperature dependent loss of the all-TiN device. We speculate that the presence of the TiN-Al interface permits the lower gap Al to act like a quasiparticle trap for the TiN.²² While quasiparticles in the Al cannot transit to the TiN due to its larger energy gap, quasiparticles generated in the TiN can traverse the interface to the Al, be trapped there and perhaps generate additional loss by subsequently generating additional quasiparticles in the Al. Presumably a similar interfacial effect would be visible in the hybrid L devices, but the comparatively small interface loss term would difficult to distinguish from the roughly 100× larger loss measured in the Al inductors.

In summary, we have shown that the measured losses as a function of power and temperature can be varied by the replacement of Al for TiN in different parts of the resonant circuit. When the lossier Al is placed in capacitive parts of the circuit, the increased TLS loss indicates that the TLSs couple to the capacitive parts of the circuit. However while the Al in the inductor has much less TLS loss, it leads to additional power independent and temperature dependent loss terms. The power independent loss is proportional to the product of the Al area × inductance and likely arises from quasiparticles generated by stray light from the 4K stage. The temperature dependent loss is related to the Al inductance and is likely from thermally activated quasiparticles. While there is an incremental interface loss between the TiN and Al at higher temperatures, $\delta_{\text{interface}} \leq 1 \times 10^{-6}$ at the base temperature. This lack of interface loss does not preclude future hybrid devices from having low losses. This work suggests that future devices can be designed with their individual circuit elements optimally tuned for their purpose, e.g., low TLS loss, superconducting gap, kinetic inductance, detection efficiency, etc., specifically tuned.^{12,23}

The authors gratefully acknowledge the assistance of F. Farhoodi and valuable discussions with J. Gao, R. Simmonds, J. Aumentado, and J. Whittaker. This work was supported by the NIST Quantum Information initiative and in part by DARPA. The views and conclusions contained in

this document are those of the authors and should not be interpreted as representing the official policies, either expressly or implied, of the U.S. Government.

- ¹P. K. Day, H. G. LeDuc, B. A. Mazin, A. Vayonakis, and J. Zmuidzinas, *Nature (London)* **425**, 817 (2003).
- ²M. Mariani, H. Wang, T. Yamamoto, M. Neeley, R. C. Bialczak, Y. Chen, M. Lenander, E. Lucero, A. D. O'Connell, D. Sank, M. Weides, J. Wenner, Y. Yin, J. Zhao, A. N. Korotkov, A. N. Cleland, and J. M. Martinis, *Science* **334**, 61 (2011).
- ³J. Gao, M. Daal, J. M. Martinis, A. Vayonakis, J. Zmuidzinas, B. Sadoulet, B. A. Mazin, P. K. Day, and H. G. LeDuc, *Appl. Phys. Lett.* **92**, 212504 (2008).
- ⁴A. D. O'Connell, M. Ansmann, R. C. Bialczak, M. Hofheinz, N. Katz, E. Lucero, C. McKenney, M. Neeley, H. Wang, E. M. Weig, A. N. Cleland, and J. M. Martinis, *Appl. Phys. Lett.* **92**, 112903 (2008).
- ⁵R. Barends, N. Vercruyssen, A. Endo, P. J. de Visser, T. Zijlstra, T. M. Klapwijk, P. Diener, S. J. C. Yates, and J. J. A. Baselmans, *Appl. Phys. Lett.* **97**, 023508 (2010).
- ⁶R. Barends, N. Vercruyssen, A. Endo, P. J. de Visser, T. Zijlstra, T. M. Klapwijk, and J. J. A. Baselmans, *Appl. Phys. Lett.* **97**, 033507 (2010).
- ⁷M. S. Khalil, F. C. Wellstood, and K. D. Osborn, *IEEE Trans. Appl. Supercond.* **21**, 879 (2011).
- ⁸M. R. Vissers, J. Gao, D. S. Wisbey, D. A. Hite, C. C. Tsuei, A. D. Corcoles, M. Steffen, and D. P. Pappas, *Appl. Phys. Lett.* **97**, 232509 (2010).
- ⁹H. G. LeDuc, B. Bumble, P. K. Day, B. H. Eom, J. Gao, S. Golwala, B. A. Mazin, S. McHugh, A. Merrill, D. C. Moore, O. Noroozian, A. D. Turner, and J. Zmuidzinas, *Appl. Phys. Lett.* **97**, 102509 (2010).
- ¹⁰S. Hunklinger and W. Arnold, *Physical Acoustics* (Academic, New York, 1976), Vol. 12, chap. 3, p. 155.
- ¹¹D. P. Pappas, M. R. Vissers, D. S. Wisbey, J. S. Kline, and J. Gao, *IEEE Trans. Appl. Supercond.* **21**, 871 (2011).
- ¹²J. M. Martinis, K. B. Cooper, R. McDermott, M. Steffen, M. Ansmann, K. D. Osborn, K. Cicak, S. Oh, D. P. Pappas, R. W. Simmonds, and C. C. Yu, *Phys. Rev. Lett.* **95**, 210503 (2005).
- ¹³H. Paik, D. I. Schuster, L. S. Bishop, G. Kirchmair, G. Catelani, A. P. Sears, B. R. Johnson, M. J. Reagor, L. Frunzio, L. I. Glazman, S. M. Girvin, M. H. Devoret, and R. J. Schoelkopf, *Phys. Rev. Lett.* **107**, 240501 (2011).
- ¹⁴H. Wang, M. Hofheinz, J. Wenner, M. Ansmann, R. C. Bialczak, M. Lenander, E. Lucero, M. Neeley, A. D. O'Connell, D. Sank, M. Weides, A. N. Cleland, and J. M. Martinis, *Appl. Phys. Lett.* **95**, 233508 (2009) and supplementary material.
- ¹⁵A. D. Corcoles, J. M. Chow, J. M. Gambetta, C. Rigetti, J. R. Rozen, G. A. Keefe, M. B. Rothwell, M. B. Ketchen, and M. Steffen, *Appl. Phys. Lett.* **99**, 181906 (2011).
- ¹⁶R. Barends, J. Wenner, M. Lenander, Y. Chen, J. Bialczak, J. Kelley, E. Lucero, P. O'Malley, M. Mariani, D. Sank, H. Wang, T. C. White, Y. Yin, J. Zhao, A. N. Cleland, J. M. Martinis, and J. J. A. Baselmans, *Appl. Phys. Lett.* **99**, 113507 (2011).
- ¹⁷M. R. Vissers, J. S. Kline, J. Gao, D. S. Wisbey, and D. P. Pappas, *Appl. Phys. Lett.* **100**, 082602 (2012).
- ¹⁸M. Sandberg, M. R. Vissers, J. S. Kline, M. Weides, J. Gao, D. S. Wisbey, and D. P. Pappas, *Appl. Phys. Lett.* **100**, 262605 (2012).
- ¹⁹G. Stan, S. B. Field, and J. M. Martinis, *Phys. Rev. Lett.* **92**, 097003 (2004).
- ²⁰O. Noroozian, J. Gao, J. Zmuidzinas, H. G. LeDuc, and B. A. Mazin, *AIP Conf. Proc.* **1185**, 148 (2009).
- ²¹J. J. A. Baselmans and S. J. C. Yates, *AIP Conf. Proc.* **1185**, 160 (2009).
- ²²K. M. Lang, S. Nam, J. Aumerntado, C. Urbina, and J. M. Martinis, *IEEE Trans. Appl. Supercond.* **13**, 989 (2003).
- ²³M. P. Weides, J. S. Kline, M. R. Vissers, M. O. Sandberg, D. S. Wisbey, B. R. Johnson, T. A. Ohki, and D. P. Pappas, *Appl. Phys. Lett.* **99**, 262502 (2011).